Developing a novel inhibitor for Cdc14 in the fungus *Aspergillus niger*

Stephanie Zhang

ABSTRACT

Fungal pathogens are a major cause of crop damage. In these fungi, Cdc14 could be a critical phosphatase for regulating cell division by ending the mitotic process, as demonstrated by studies in *Saccharomyces cerevisiae*. Due to Cdc14's absence in higher plants and noncritical role in animals, an inhibitor which can reduce its activity could function as a potential fungicide.

In this project, I developed an inhibitor for Cdc14 in the fungal pathogen *Aspergillus niger* (AnCdc14), a pathogen that causes black mold on crops. After characterizing the catalytic specificity of AnCdc14, I designed multiple inhibitors that modeled the specificity. A combination of bioinformatic and biochemical approaches was used to determine the most effective inhibitor: one that contained four benzene rings and functioned through irreversible inhibition. Through computer modeling, I optimized this inhibitor to improve its affinity for AnCdc14. This modified inhibitor can be tested *in vitro* and *in vivo* for its efficiency in preventing *A. niger* growth and eliminating its pathogenicity.

Due to high conservation of Cdc14 among fungi species, the inhibitor I created could be tested in multiple fungi, such as *F. graminearum*. Eventually, these results could be developed into a new antifungal compound that broadly prevents plant fungal infections.

INTRODUCTION

Every year, fungal pathogens destroy more than 125 million tons of food, enough to feed 600 million people (1). Fungicides are a common method to control these fungal damages, but fungi inevitably evolve resistance to these chemicals. Therefore, there exists a long felt yet unfulfilled need to find new, effective, and economic fungicides. One path to find new fungicides is to find molecules that inhibit a biological process necessary for fungi growth and pathogenesis.

Molecules that inhibit the enzyme Cdc14 are great candidates for such a purpose because Cdc14 is essential for fungal development. Cdc14 in *Saccharomyces cerevisiae* (*S. cerevisiae*) has been researched extensively and shown to dephosphorylate its substrates. It plays a major role in the Mitotic Exit Network by inactivating cyclin-dependent kinases (CDKs), thereby ending mitosis and regulating cytokinesis (2,3) (Figure 1). When ScCdc14 is inhibited or not present, the cell is unable to finish mitosis and therefore unable to develop properly (4). Studies also demonstrate that ScCdc14 helps to coordinate DNA repair and genome stability (5).

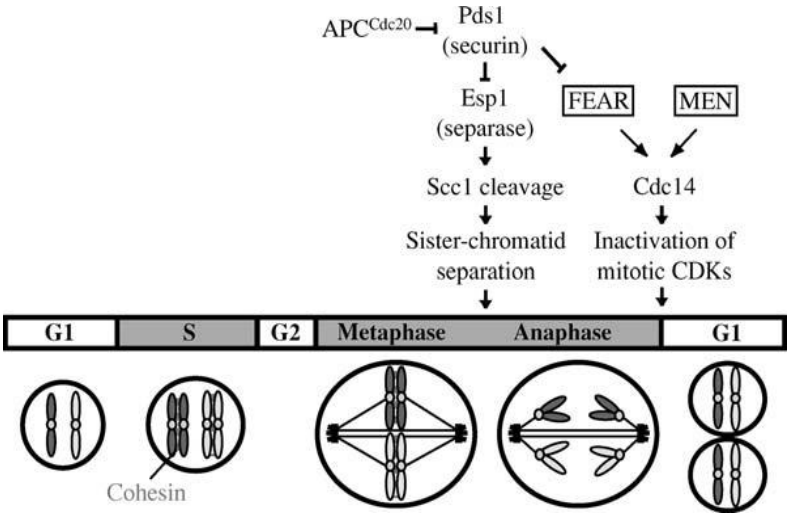

Figure 1. Regulation of mitosis in *S. cerevisiae*: Cdc14 promotes mitotic exit by antagonizing mitotic CDK activity. The activity of Cdc14 is regulated by two signaling pathways, the Cdc14 early anaphase release (FEAR) network and the mitotic exit network (MEN). Diagram from Source 4.

Cdc14 is an attractive target for antifungal drug development for several other important reasons. First, genetic deletion of Cdc14 severely retards growth and eliminates pathogenicity of *Fusarium graminearum* (*F. graminearum*) and *Magnaporthe oryzae* (*M. oryzae*) (6,7). Second, catalytic sequences of all Cdc14 orthologs in different fungi species are highly conserved, indicating that these orthologs had similar substrate specificity (8). This makes design of competitive inhibitors for a broad family of fungi achievable. Third, *Cdc14* phosphatase genes are conserved in fungi but are absent from higher plants (9). Genetic studies indicate its function in animal and human cells is not critical, contradicting its function in fungal cells (10). Thus, plants or consuming animals and humans are likely to be unaffected by compounds that specifically inhibit Cdc14.

Aspergillus niger (*A. niger*), is a fungus that causes black mold on certain crops, fruits, and vegetables such as rice, grapes, apricots, onions, and peanuts. *A. niger* produces Ochratoxin A, a toxin that can pose a major health hazard to both humans and animals (11). Therefore, developing a fungicide that can control the *A. niger* pathogenic infection has both economic and health values.

In this study, I characterized the catalytic specificity for Cdc14 in *A. niger* (AnCdc14) and found that optimal substrates for AnCdc14 contain the amino acid sequence phosphorylated serine (Ser(P))-proline (P)-X (any amino acid)-lysine or arginine (Lys/Arg). This is similar to the specificity for other Cdc14 orthologs, such as Cdc14 in *S. cerevisiae* (ScCdc14), Cdc14 in *F. graminearum* (FgCdc14), and Cdc14 in *M. oryzae* (MoCdc14), suggesting that inhibitors that are efficient on AnCdc14 could also inhibit its orthologs and vice versa.

An initial screening of 10,000 potential Cdc14 inhibitors at the Bindley Bioscience Center has identified 13 lead inhibitors of ScCdc14 (see Table S2 in the appendix). To look for

competitive inhibitors that are highly specific for the Cdc14 family but broadly reactive across fungal species, I tested these 13 inhibitors and selected the most efficient one for AnCdc14 using computer modeling as well as a standard phosphatase assay and an IC50 curve. The IC50 value generated from this curve is the concentration of an inhibitor needed to reduce biological activity by half; it is a measurement for drug efficiency and is commonly used in pharmacological research.

With a combination of *in vitro* and *in silico* techniques, I modified and optimized this inhibitor to ultimately create an improved inhibitor for AnCdc14. This "generation two" molecule has the potential to inhibit AnCdc14 and broadly act against all fungi orthologs of Cdc14, thus making it a good candidate for a future fungicide.

MATERIALS AND METHODS

Transformation and Purification

Purified *AnCdc14* DNA was inserted into the plasmid pET15b (produced by Genscript) between the NdeI and BamHI restriction sites. This created a fusion on the 5' end of the *AnCdc14* with the 6xHis tag sequence. This sequence ultimately allowed for isolation and purification of the target protein by nickel affinity chromatography.

The genetically modified plasmid was then transformed into competent *Escherichia coli (E. coli)* BL21 AI cells with the heat shock method. DNA was mixed with the bacteria cells and placed in 42 °C for one minute, then in ice, then in 37 °C incubation for 30 minutes (12). The transformed bacteria were selected by ampicillin (as the original plasmid contained an ampicillin-resistant maker) and then amplified overnight.

Harvested bacteria were lysed on ice for 30 min in lysis buffer (25mM HEPES pH7.5, 500 mM NaCl, 0.1% (v/v)Triton x-100, 10 mM imidazole, 10% (v/v) glycerol) supplemented with 50 mg/mL Lysozyme,10 μM Leupeptin, 1 μM Pepstatin, and universal Nuclease. The bacteria were sonicated to reduce viscosity. After centrifugation at 35,000 g for 30 min at 4°C, the resulting soluble extract was used to run AKTA chromatography. During the chromatography, proteins with a Histidine tag bound to the nickel column and were then washed with imidazole. The imidazole was later dialyzed away, leaving just purified proteins.

A Bradford Assay was performed with the purified protein to measure the concentration using a standard curve. SDS-Page gel electrophoresis was run for one hour at 180 volts with a running gel containing 30% acrylamide with a cross-linking ratio of 29:1. This gel was set in Coomassie blue staining solution before being imaged with Bio-Rad Gel Doc EZ imaging

system and analyzed with ImageLab. The molecular weight of the protein confirmed that the purified protein was AnCdc14.

Phosphatase Assays

To confirm that AnCdc14 had tyrosine phosphatase activity, phosphatase reactions were conducted. Sodium orthovanadate inhibits all tyrosine phosphatases and was added at three concentrations (0, 500, and 1000 μM) to a solution of 0.3 μM of AnCdc14 and 300 mM of artificial substrate pNPP. The amount of dephosphorylated pNPP (p-nitrophenol, or pNP) produced from each of the three reactions was calculated using a standard pNP curve.

To determine necessary concentrations and time needed to achieve steady state conditions, 30 mM of pNPP and 0.3 μM of AnCdc14 were incubated for 60 minutes at 24 °C. Absorbance values at 405 nm determined the amount of pNP produced and were measured every minute. The results indicated that 20 minutes at 30 °C was sufficient to reach steady state with 0.3 μM of AnCdc14 and 30 mM of pNPP.

A Michaelis-Menten assay was then performed to ensure that future assays would be under steady-state conditions, to determine the average initial velocity of the reaction, and to find the values for k_{cat} and K_m in AnCdc14. This assay was performed with various concentrations of the substrate pNPP (1, 3, 6, 12.5, 30, and 50 mM) and 0.3 μM AnCdc14 for 20 minutes at 30 °C. The results were graphed on ImageLab and fitted to the Michaelis-Menten equation.

Catalytic Specificity

AnCdc14's catalytic ability to dephosphorylate 24 artificial substrates (Table S1) with different amino acid sequences was tested to determine AnCdc14's catalytic specificity (13). 100 μM of each substrate were mixed with 0.13 μM of AnCdc14 for 20 minutes at 30 °C (an additional phosphatase assay determined these conditions necessary to reach steady state). The

amount of phosphate released from each reaction was calculated using a standard curve for BioMol Green, which reacts with free phosphate, and the results were plotted on a bar graph to determine AnCdc14's catalytic specificity.

In silico *Inhibition of AnCdc14*

A model of AnCdc14's protein structure was made based on the corresponding amino acid sequence and the known crystal structure of ScCdc14: 5XW4. This homology model was built using Phyre2, a suite of software tools to predict and analyze protein structure, function, and mutations (14). 3D Ligand Site, a specific tool of Phyre2, was used to find the binding site of the homology model (15). Specific inhibitor molecules (Table S2) were docked into the model's catalytic site using MCule's 1-Click Docking tool, a website that docks inhibitors and generates values that represent binding affinity ("S" scores). The inhibitors were docked at the position Arg188_C1279, which corresponded to the point X: 38.973, Y: -0.664, Z: 4.359 in the homology model. The S values were graphed in a bar graph to predict results for the *in vitro* inhibition assays.

In vitro *Inhibition of AnCdc14*

The same 13 inhibitors (Table S2) were tested *in vitro* to find the accuracy and validity of the homology model and to determine the most efficient inhibitor for AnCdc14. 50 μM of each inhibitor were mixed with 30 mM of pNPP and 0.3 μM AnCdc14. From this assay, three inhibitors were determined to be the most effective and have the highest binding affinity for AnCdc14, thus producing less product.

Each of these three inhibitors were used to plot an IC_{50} curve at concentrations of 0, 0.25, 0.5, 1, 2, 5, 10, 25, 50, 100, and 200 μM with 30 mM pNPP and 0.3 μM AnCdc14. The

IC_{50} value and K_i value were determined for each of these inhibitors. From these assays, the best inhibitor was identified and was used in further experiments.

Mechanism of Inhibition

To determine the mechanism of inhibition that the top inhibitor used, Michaelis-Menten curves were created for three different inhibitor concentrations: 0, 2.5, and 10 μM. These inhibitors were tested at pNPP concentrations of 1, 2, 5, 10, 25, 50, 75, and 100 mM with 0.6 μM AnCdc14 for 20 minutes at 30 °C. The three curves were graphed on ImageLab and fitted to the Michaelis-Menten equation.

To test for reversibility of inhibition, 10 μM of inhibitor and 0.6 μM of enzyme were incubated at 25 °C for 0, 15, and 30 minutes. Following the incubation time, 30 mM of pNPP was added and incubated for 20 minutes at 30 °C.

Optimization of Inhibitor in silico

The identified best inhibitor was optimized in MCule's 1-Click Docking. The site's construction tool was used to add structures to the original inhibitor to increase its binding affinity for AnCdc14 and thus produce a better inhibitor.

RESULTS AND DISCUSSION

Transformation and Purification

After inducing expression of AnCdc14 in E. coli, I extracted proteins from the transformed cells and ran nickel affinity chromatography to purify the AnCdc14 enzyme. The UV absorbance trace from the AKTA purification system showed a large peak where there was a high imidazole concentration, suggesting reaction tubes 20 through 30 contained the protein (Figure 2A).

To ensure that the purified protein was AnCdc14, I ran gel electrophoresis using a fraction of purified protein sample. A thick band at 51.0 kDa, very close to calculated size of 52.2 kDa based on amino acid sequence, suggested that I isolated the correct protein (Figure 2B).

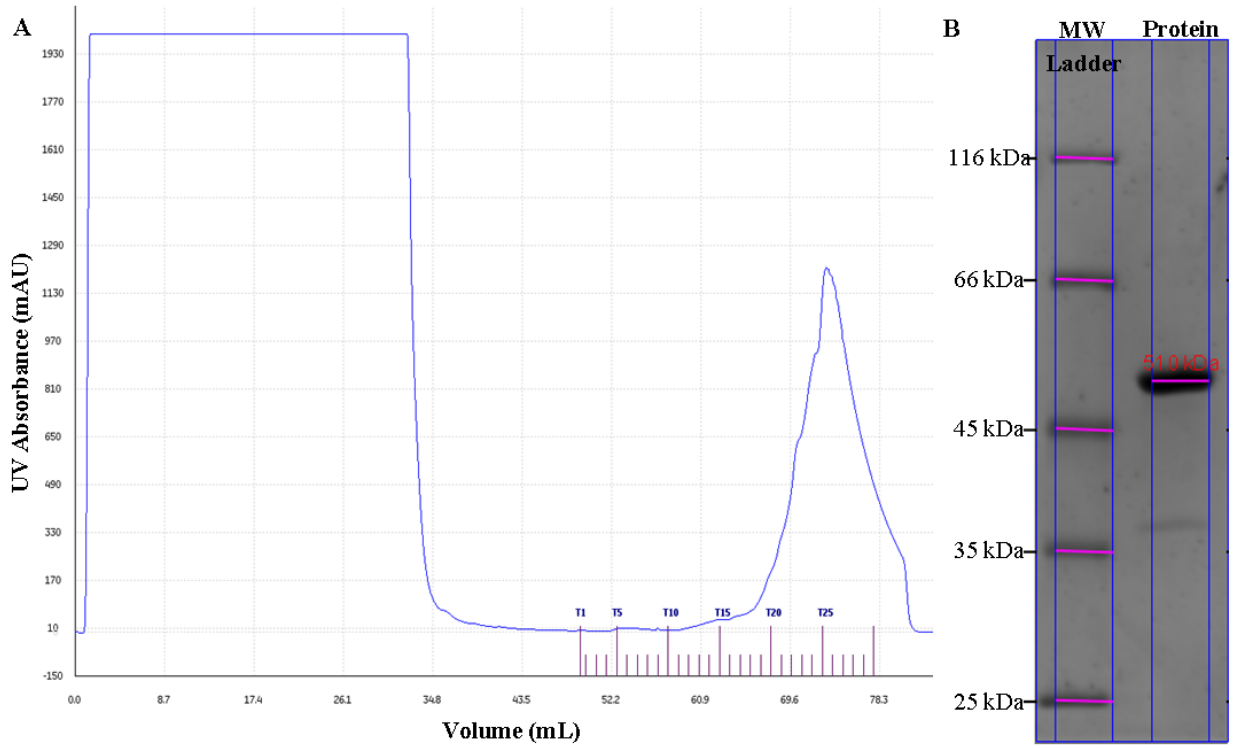

Figure 2. Purification of AnCdc14: A. The UV absorbance signal during the AKTA purification run for each volume of sample that passed through the column suggests successful purification of protein. The large spike in absorbance signifies which samples from the AKTA system contained the highest concentration of imidazole. **B.** SDS-Page gel analysis using Coomassie blue staining demonstrates a thick band of AnCdc14 at 51.0 kDa.

With purified AnCdc14, I performed a Bradford assay (data not shown) to find that the AnCdc14 concentration was 129.5 µM.

Phosphatase Assays

Phosphatase activity of AnCdc14 was confirmed by an assay using sodium orthovanadate (a protein tyrosine phosphatase inhibitor) as an inhibitor and pNPP (an artificial small molecule) as the substrate. The results demonstrated that at inhibitor concentration of 500 µM, percent inhibition increased slightly, from 0% to 7.3%; at inhibitor concentration of 1000 µM, the percent inhibition increased at a much greater magnitude, from 7.3% to 40.5% (Figure 3A). The result indicated that increased concentrations of phosphatase inhibitor decreased AnCdc14 activity. The sodium orthovanadate assay confirmed AnCdc14's phosphatase activity, and I found the enzyme's specific activity to be 6.51 min^{-1}.

In the reaction of AnCdc14 with pNPP, I found that the graph was linear for the first 40 minutes (Figure 3B). Because the linear portion of the graph represented when my enzyme was in the steady state, I determined that all further experiments conducted with steady state properties would have to be conducted in less than 40 minutes.

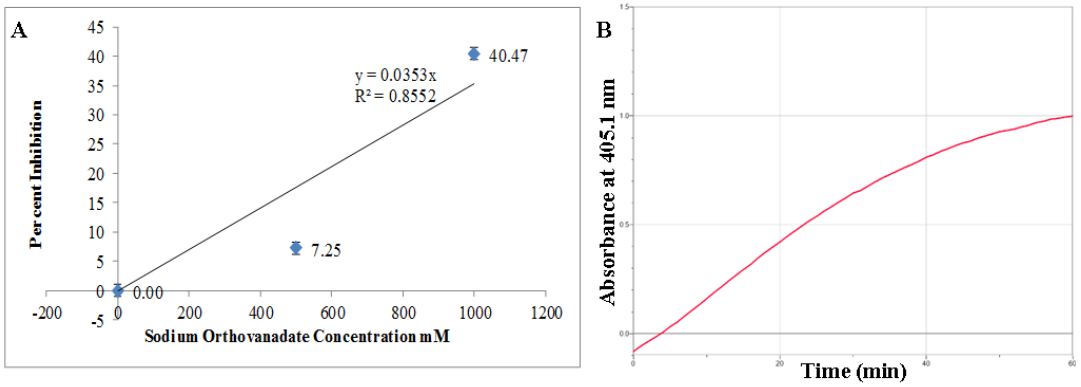

Figure 3. AnCdc14 Phosphatase Activity and Steady State Conditions: A. Sodium orthovanadate, a protein tyrosine phosphatase inhibitor, was added to AnCdc14 at various concentrations. Percent inhibition increased with increased concentration of the inhibitor. The error bars shown are standard deviations for the three trials I completed. **B.** Shown is absorbance at 405.1 nm over 60 minutes as AnCdc14 reacted with the substrate pNPP. The absorbance is a measure representative of the amount of phosphate produced from the AnCdc14 catalyzed reaction.

With the steady-state time parameter determined, I calculated k_{cat} and K_m values for AnCdc14 using a Michaelis-Menten curve. The curve yielded that the K_m value was 72.25 mM, v_{max} was 16.64 µM/min, and k_{cat} was 0.92 sec^{-1} (Figure 4). These values were used in future experiments to calculate k_{cat}/K_m and K_i values.

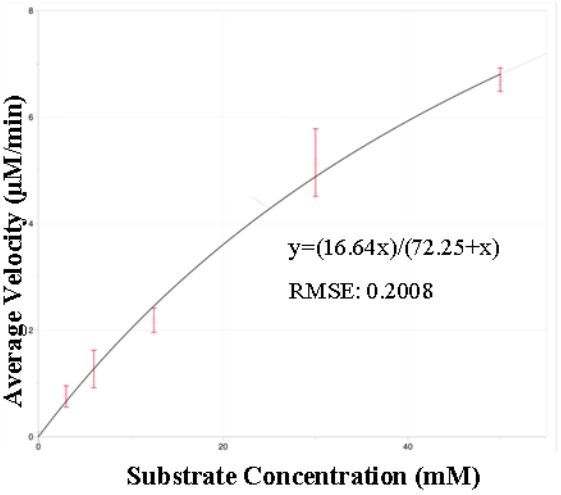

Figure 4. Michaelis-Menten Curve with the Substrate pNPP: The average velocity of product produced in µM per minute for each of the substrate concentrations were fit to a Michaelis-Menten curve. The velocity of the phosphate produced was calculated using the absorbance values of the reactions after 20 minutes of reacting at 30 °C. The error bars shown represent standard deviation over the three conducted trials, and the curve was generated by ImageLab and is fit by the Michaelis-Menten equation: velocity=(v_{max}*[substrate])/(K_m+[substrate]).

Catalytic Specificity

To find the AnCdc14 substrate specificity, I selected 24 substrates (Table S1) and tested catalytic efficiency of AnCdc14 on them. These 24 substrates were selected based on previous studies with ScCdc14 and other Cdc14 family members (2).

I measured the amount of phosphate that was produced by each substrate reaction catalyzed by AnCdc14. These values were used to calculate the k_{cat}/K_m values for each substrate. Higher quotients indicate substrates with higher binding affinity to AnCdc14. Substrates #1, #7, and #24 were found to be the best substrates and #8, #9, #14, and #17 were shortly behind (Figure 5). Upon comparison of the corresponding sequences, I found that these sequences shared a phosphorylated serine group followed by a proline in the +1 position and a lysine in the

+3 position (Table S1). This sequence was absent at the substrates showing low AnCdc14 binding affinity, such as #10, #11, #12, #13, and it also matched the highly conserved substrate specificity among other Cdc14 family members, including ScCdc14 (16).

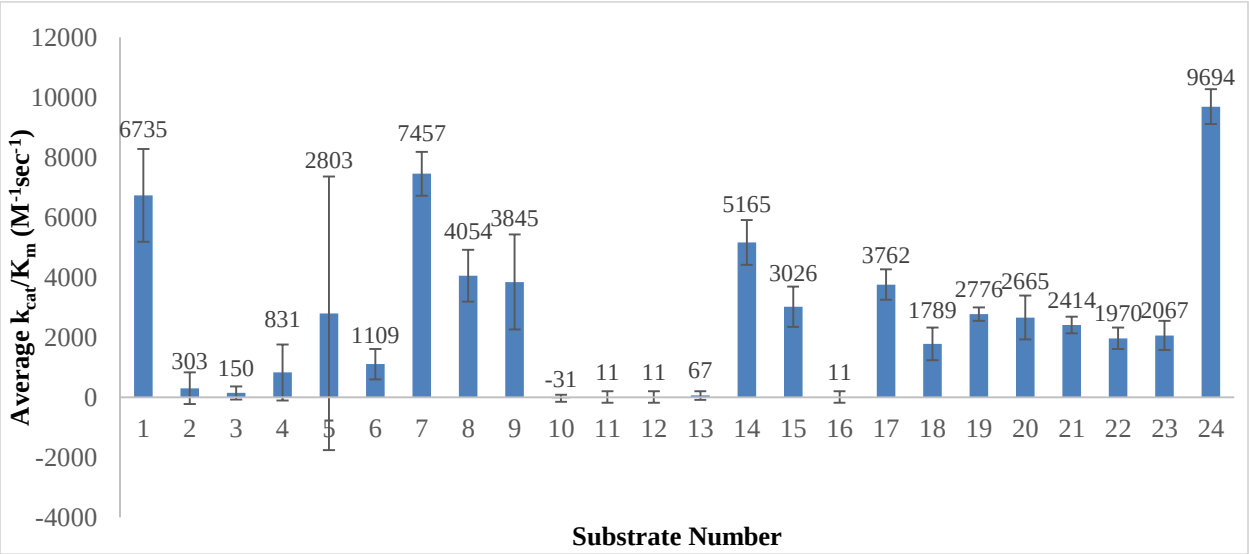

Figure 5. Substrate Specificity of AnCdc14: The average k_{cat}/K_m values for each substrate were used to compare substrate sequences and determine catalytic specificity of AnCdc14. The error bars on the graph indicate the standard deviations among the three trials. The substrates corresponding to the numbers on the x-axis can be found in Table S1 (in the appendix).

In silico *Inhibition of AnCdc14*

Due to limited research on AnCdc14's protein structure, I had to develop a model of it based on ScCdc14's crystal structure and AnCdc14's gene sequence (Figure 6A). With my homology model, I tested 13 pre-screened inhibitors to predict their efficiency. These inhibitors were designed and selected based on the specificity of ScCdc14. I docked each of these inhibitors into AnCdc14's active site via the computer software program "1-Click Docking." This procedure produced an S score that represented the binding affinity of the inhibitor for the enzyme. S scores with higher absolute values represented higher binding affinity. Though many of the inhibitors had similar S scores, inhibitors #2 and #4 (Table S2) were marginally better than the others in terms of S score, with inhibitors #1, #3, and #6 following (Figure 6C). Inhibitor #4

is shown docked in Figure 6B at the active site, Arg188, which was determined by 3D Ligand Site.

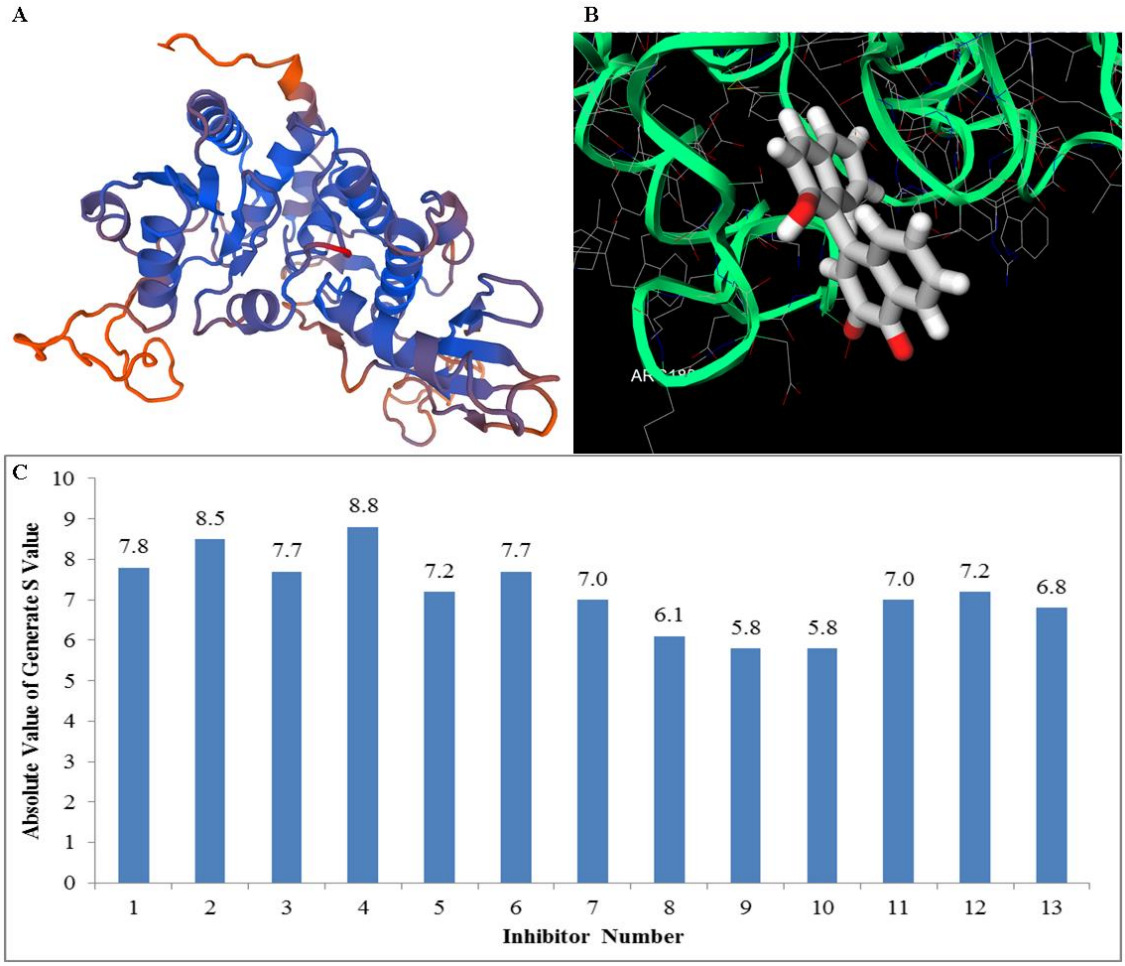

Figure 6. Docking Inhibitors for AnCdc14: A. The homology model of AnCdc14 was developed based on the structure of ScCdc14. Shown are the predicted alpha helices and beta sheets. The section highlighted in red at the front of the model represents the active site, Arg188. **B.** Inhibitor #4, which was deemed to be the best inhibitor by comparison, docked to the homology model at the active site. **C.** The absolute values of the S values generated by 1-Click Docking are graphed for each inhibitor to compare binding affinity for the 13 inhibitors. The inhibitor molecules corresponding to the numbers on the x-axis can be found in Table S2 (in the appendix).

In vitro *Inhibition of AnCdc14*

To validate the prediction made by 1-Click Docking, *in vitro* assays with each inhibitor were performed and the inhibition percentage was calculated for each inhibitor. In line with the predictions, inhibitors #1, #3, and #4 were AnCdc14's top inhibitors, with number 4 being the most effective (Figure 7A).

From the IC_{50} curve equations generated from the assays, I found that the IC_{50} values for inhibitors #1, #3, and #4 were 31.9, 9.1, and 7.5 µM (Figures 7B, 7C, 7D). Inhibitor #4 had the smallest IC_{50} value, indicating that it required the smallest concentration to inhibit AnCdc14 by 50%, thus it is the most efficient inhibitor. These results also supported the inhibitor assay results discussed in the previous paragraph (Figure 7A).

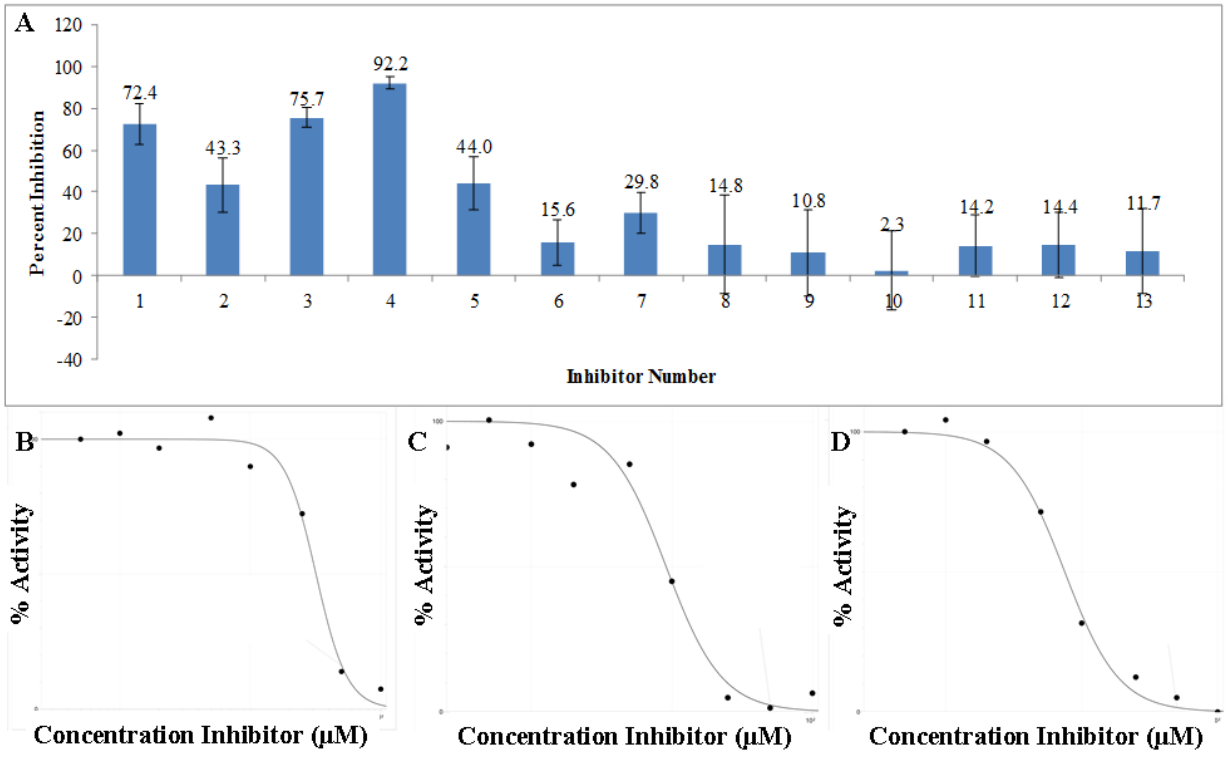

Figure 7. *In vitro* Inhibition of AnCdc14: A. The percent inhibition for each of the compounds was used to determine the best inhibitors. The error bars represent standard deviation among the three trials. The compounds associated with each inhibitor number on the x-axis can be found in Table S2 (in the appendix). **B-D.** IC_{50} curves for inhibitors #1, #3, and #4 (respectively). The R^2 values of these curves were 0.9939, 0.964, and 0.9827, respectively. The data were analyzed via nonlinear curve fitting in the "My Curve Fit" software, using the IC_{50} formula: y=100/(1+(x/ IC_{50})^cooperativity).

Using inhibitor #4's IC_{50} value as well as AnCdc14's K_m value, K_i was calculated to be 5.3 µM, the inhibitor concentration required to bind half of the enzyme molecules.

In addition, from the IC50 curves, I found that the cooperativity values for inhibitor #3 and #4 were 2.18 and 2.17, respectively, suggesting that AnCdc14 acted as a dimer (two

catalytically active sites). This was further supported by the fact that the R^2 values increased considerably when the cooperativity factor was added into the IC50 equation. This is also consistent with studies of other Cdc14 family members, as ScCdc14 is also a homo-dimer.

Mechanism of Inhibition

To determine which method of inhibition the inhibitor #4 actually employed, two concentrations of inhibitor #4 were used in the mechanism assay (Figure 8A, Table 1). I found that both K_m and v_{max} changed, suggesting the mechanism of inhibition to be mixed: both competitive (higher K_m) and noncompetitive (lower v_{max}).

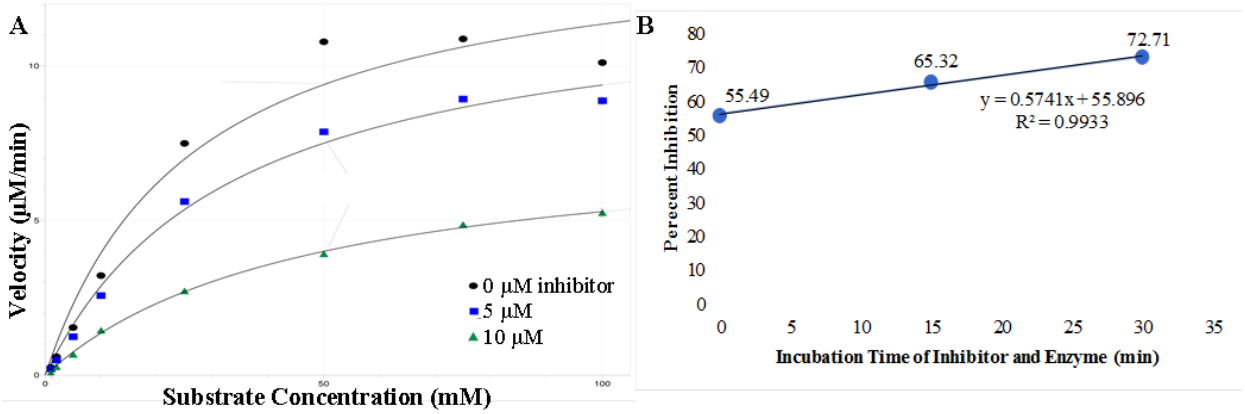

Figure 8. AnCdc14 is Inhibited Irreversibly: **A.** The average initial velocity of phosphate produced for different substrate concentrations from two trials created Michaelis-Menten curves. Inhibitor concentrations used for the different curves were 0 µM (black), 2.5 µM (blue), and 10 µM (green). The curves were generated by ImageLab and are fit by the Michaelis-Menten equation: velocity=(v_{max}*[substrate])/(K_m+[substrate]).**B.** Percent inhibition graphed for different amounts enzyme and inhibitor incubation times shows that inhibitor #4 is an irreversible inhibitor. The line of best fit shown has an equation of y=0.5741x+55.896, and the R^2 value is 0.9933, representing a strong correlation.

Table 1. v_{max} and K_m Results for Mechanism of Inhibition Assay: The v_{max} and K_m values were calculated from the Michaelis-Menten curves and their equations for each concentration of inhibitor.

[Inhibitor] (µM)	v_{max} (µM/min)	K_m (mM)
0.00	14.31	26.30
2.50	12.52	33.46
10.00	7.78	47.16

However, another potential explanation for these data was that AnCdc14 was inhibited irreversibly. Irreversible inhibition occurs when the inhibitor remains covalently bound to the enzyme's active site, making it unable to bind more substrates and thereby lose its catalytic function (Figure 9). One criterion used to identify irreversible inhibitors is showing that percentage inhibition increases over time. By incubating inhibitor #4 with AnCdc14, I received results that showed 55.5% inhibition at 0 minute, 65.32% inhibition at 15 minute, and 72.71% inhibition at 30 minute (Figure 8B). These data suggested that longer periods of time increased the percent inhibition of AnCdc14, demonstrating that AnCdc14 was inhibited irreversibly by inhibitor #4.

The irreversible inhibition mechanism was further supported by two sets of previously discussed results: the binding affinity for inhibitor #4 on AnCdc14 was high (Figure 7A) and inhibitor #4's molecular structure fit well into my homology model's binding site (Figure 6B). Both suggested that inhibitor #4 might be able to covalent bonds as an irreversible inhibitor rather than hydrogen bonds as a reversible inhibitor.

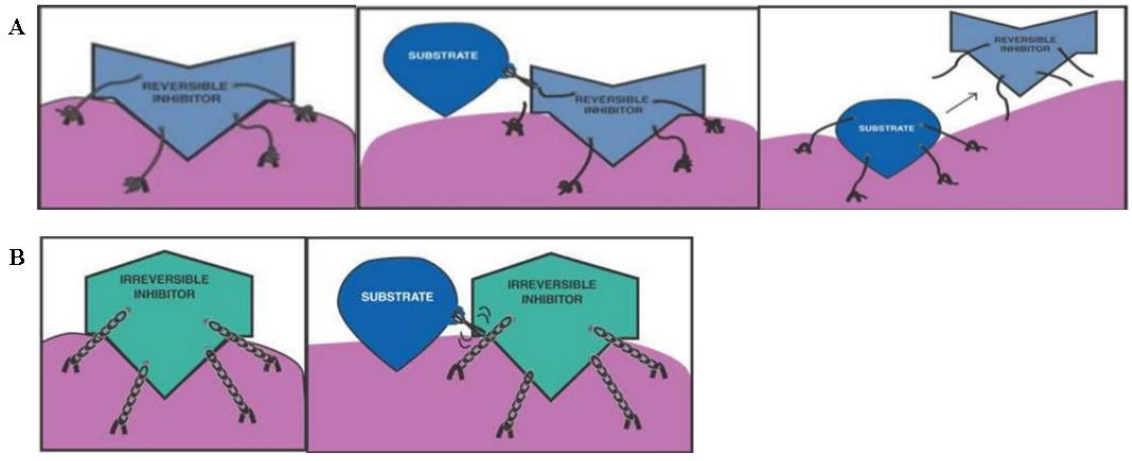

Figure 9. Diagrams of Inhibition Mechanisms: A. A reversible inhibitor binds to an enzyme in either the active site (competitive inhibition) or another site (noncompetitive inhibition). This temporarily blocks the substrate from binding to the enzyme but does not permanently disable enzyme activity. **B.** An irreversible inhibitor binds to the active site of an enzyme and creates covalent bonds, thus permanently disabling the enzyme and not allowing substrates to bind. Diagrams from Source 17.

Optimization of Inhibitor in silico

Both *in silico* and *in vitro* test suggested that inhibitor #4 was the best inhibitor. Using 1-Click Docking, I was able to change and optimize inhibitor #4 for increased binding affinity for AnCdc14. Such changes involved adding one more benzene ring, adding chlorine to create more intermolecular bonds with the hydrogens in the catalytic site, and adding a hydroxyl group to increase the number of hydrogen bonds (Figure 10A). Specifically, the binding affinity of inhibitor to AnCdc14 increased, with a change in absolute value of S value from 8.8 to 9.8. The optimized inhibitor can be seen docked into the AnCdc14 homology model in Figure 10B.

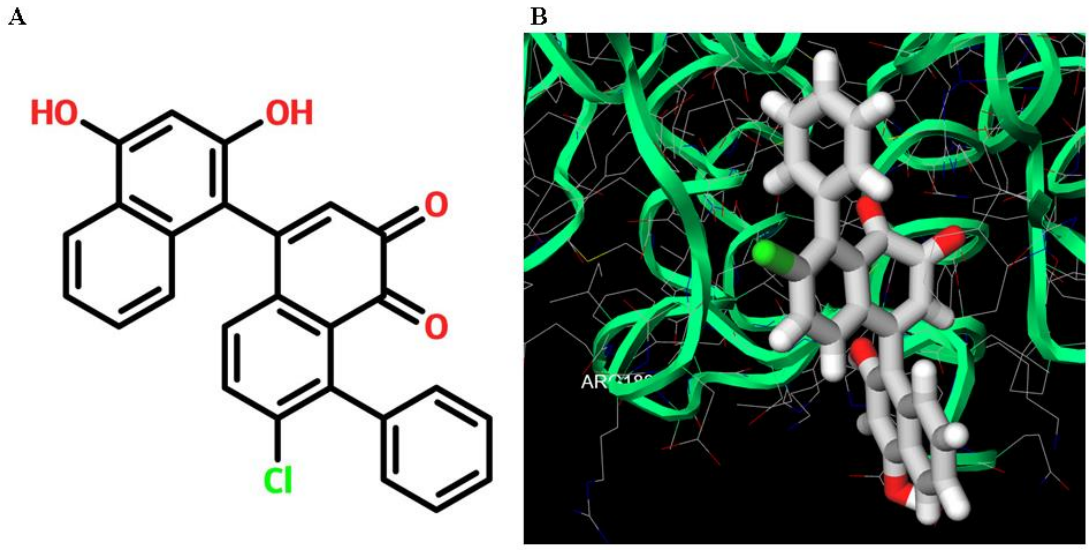

Figure 10. Optimized Inhibitor #4: **A.** The structure of inhibitor #4 was slightly changed in order to increase binding affinity for the active site of AnCdc14. A benzene ring and a Chlorine group were added to the original structure. **B.** The optimized inhibitor docked in the active site had a higher binding affinity, with a new absolute value of S value as 9.8, compared to the original S value of 8.8 Arg188, the binding site, is labeled in the figure.

CONCLUSIONS AND FUTURE WORK

In this project, I demonstrated that AnCdc14 conserved the catalytic specificity of the Cdc14 family, and I developed an inhibitor that can broadly act against all fungi with a Cdc14 ortholog.

The inhibitor I developed in this project could be developed into a pesticide to act against *A. niger* and other fungal pathogens such as *F. graminearum* and *M. oryzae*. However, further studies both *in vitro* and *in vivo* are needed to confirm its ability to inhibit AnCdc14 and other Cdc14 orthologs, such as ScCdc14, FgCdc14, and MoCdc14.

A plant infection assay using this new inhibitor could be conducted to demonstrate that it can actually prevent infection from pathogens containing Cdc14 orthologs. In addition, research conducted on whether the new fungicide causes any health problem in plants and animals, especially humans, will be needed before the new inhibitor can be considered as a real fungicide candidate.

APPENDIX

Table S1. Substrate Naming Convention: The {p} represents a phosphorylated amino acid. The letters represent amino acid groups.

1	HT{pS}PIKSIG
2	HT{pT}PIKSIG
3	HT{pY}PIKSIG
4	HT{pS}AIKSIG
5	HT{pS}PIASIG
6	HT{pS}PIRSIG
7	HT{pS}PIKKIG
8	HT{pS}PKKSIG
9	HT{pS}PIKSKG
10	HT{pS}PKASIG
11	HT{pS}PIAKIG
12	HT{pS}PIASKG
13	HT{pS}PIASIK
14	AT{pS}PIKSIG
15	HA{pS}PIKSIG
16	HT{pS}KIKSIG
17	HT{pS}PEKSIG
18	HT{pS}PIKEIG
19	HT{pS}PIKSEG
20	HT{pS}PIKSIE
21	HT{pS}PIKSIK
22	KT{pS}PIKSIG
23	HK{pS}PIKSIG
24	HT{pS}PIKKRG

Table S2. Inhibitor Naming Convention.

Inhibitor Compound	Structure	Inhibitor Compound	Structure
1	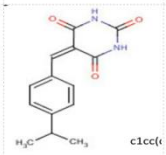	2	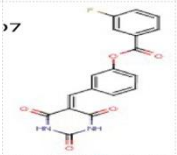
3	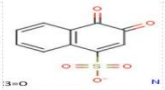	4	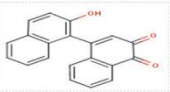
5	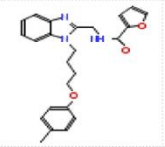	6	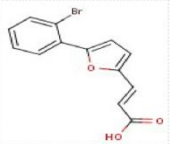
7	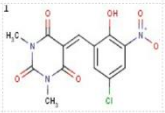	8	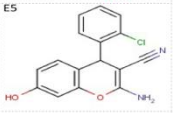
9	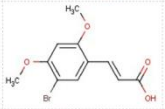	10	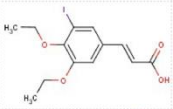
11	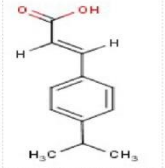	12	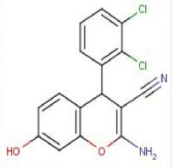
13	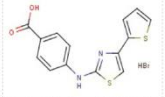		

REFERENCES

1. Fisher, M., Henk, D., Briggs, C., Brownstein, J., Madoff, L., McCraw, S., and Gurr, S. (2012) Emerging fungal threats to animal, plant and ecosystem health. *Nature* 484, 186-194.
2. Bremmer, S., Hall, H., Martinez, J., Eissler, C., Hinrichsen, T., Rossie, S., Parker, L., Hall, M., and Charbonneau, H. (2011) Cdc14 Phosphatases Preferentially Dephosphorylate a Subset of Cyclin-dependent kinase (Cdk) Sites Containing Phosphoserine. *Journal of Biological Chemistry* 287, 1662-1669.
3. Visintin, R., Craig, K., Hwang, E., Prinz, S., Tyers, M., and Amon, A. (1998) The Phosphatase Cdc14 Triggers Mitotic Exit by Reversal of Cdk-Dependent Phosphorylation. *Molecular Cell* 2, 709-718.
4. Stegmeier, F., and Amon, A. (2004) Closing Mitosis: The Functions of the Cdc14 Phosphatase and Its Regulation. *Annual Review of Genetics* 38, 203-232.
5. Eissler, C., Mazón, G., Powers, B., Savinov, S., Symington, L., and Hall, M. (2014) The Cdk/Cdc14 Module Controls Activation of the Yen1 Holliday Junction Resolvase to Promote Genome Stability. *Molecular Cell* 54, 80-93.
6. Li, C., Melesse, M., Zhang, S., Hao, C., Wang, C., Zhang, H., Hall, M., and Xu, J. (2015) FgCDC14 regulates cytokinesis, morphogenesis, and pathogenesis in Fusarium graminearum. *Molecular Microbiology* 98, 770-786.
7. Li, C., Cao, S., Zhang, C., Zhang, Y., Zhang, Q., Xu, J., and Wang, C. (2017) MoCDC14 is important for septation during conidiation and appressorium formation in Magnaporthe oryzae. *Molecular Plant Pathology.*
8. Mocciaro, A., and Schiebel, E. (2010) Cdc14: a highly conserved family of phosphatases with non-conserved functions?. *Journal of Cell Science* 123, 2867-2876.
9. Kerk, D., Templeton, G., and Moorhead, G. (2007) Evolutionary Radiation Pattern of Novel Protein Phosphatases Revealed by Analysis of Protein Data from the Completely Sequenced Genomes of Humans, Green Algae, and Higher Plants. *PLANT PHYSIOLOGY* 146, 351-367
10. Ah-Fong, A., and Judelson, H. (2011) New Role for Cdc14 Phosphatase: Localization to Basal Bodies in the Oomycete Phytophthora and Its Evolutionary Coinheritance with Eukaryotic Flagella. *PLoS ONE* 6, e16725.
11. Abarca, M. L., Bragulat, M. R., Castella, G., & Cabanes, F. J. (1994). Ochratoxin A production by strains of Aspergillus niger var. niger. Applied and environmental microbiology, 60(7), 2650-2652.
12. Froger, A., & Hall, J. E. (2007). Transformation of Plasmid DNA into E. coli Using the Heat Shock Method. *Journal of Visualized Experiments* : JoVE, (6), 253.
13. Powers, B., Melesse, M., Eissler, C., Charbonneau, H., and Hall, M. (2016) Measuring Activity and Specificity of Protein Phosphatases. *Methods in Molecular Biology*, 221-235.
14. Kelley, LA, et al. (2015) The Phyre2 web portal for protein modeling, prediction and analysis. *Nature Protocols* 10, 845-858.
15. Wass M.N., Kelley L.A. and Sternberg M.J. (2010) 3DLigandSite: predicting ligand-binding sites using similar structures. *NAR* 38, W469-73.
16. Gray, C. (2003) The structure of the cell cycle protein Cdc14 reveals a proline-directed protein phosphatase. *The EMBO Journal* 22, 3524-3535.
17. Stahl, S. (2011). Stahl's Essential Psychopharmacology: Neuroscientific Basis and Practical Applications. 4th ed. Cambridge: Cambridge University Press.

All figures and images were generated and created by Stephanie Zhang unless otherwise specified.